TU Delft

Delft University of Technology

Document Version
Final published version

Licence
CC BY-NC-ND

Citation (APA)
Ghosh Dastidar, S., Sarkar, K., Chandra, D., Hazra, B., & Vishal, V. (2025). Investigating Pore Characteristics and Their Dependence on Shale Composition: Case Study from a Permian Basin in India. *ACS Omega*, *10*(5), 4395-4405. https://doi.org/10.1021/acsomega.4c07214

Important note
To cite this publication, please use the final published version (if applicable).
Please check the document version above.

Copyright
In case the licence states “Dutch Copyright Act (Article 25fa)”, this publication was made available Green Open Access via the TU Delft Institutional Repository pursuant to Dutch Copyright Act (Article 25fa, the Taverne amendment). This provision does not affect copyright ownership.
Unless copyright is transferred by contract or statute, it remains with the copyright holder.

Sharing and reuse
Other than for strictly personal use, it is not permitted to download, forward or distribute the text or part of it, without the consent of the author(s) and/or copyright holder(s), unless the work is under an open content license such as Creative Commons.

Takedown policy
Please contact us and provide details if you believe this document breaches copyrights.
We will remove access to the work immediately and investigate your claim.

This work is downloaded from Delft University of Technology.

ACS OMEGA

Open Access

This article is licensed under CC-BY-NC-ND 4.0

http://pubs.acs.org/journal/acsodf

Article

Investigating Pore Characteristics and Their Dependence on Shale Composition: Case Study from a Permian Basin in India

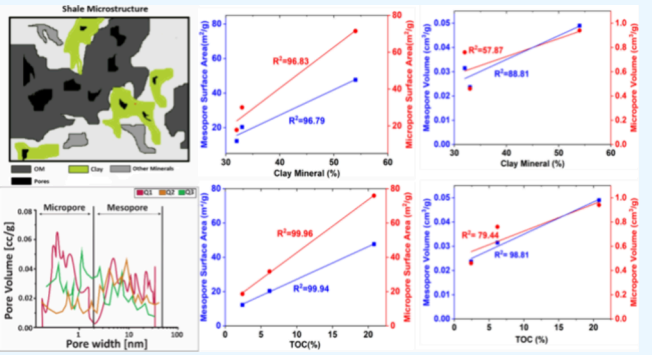
Saheli Ghosh Dastidar, Kripamoy Sarkar, Debanjan Chandra, Bodhisatwa Hazra, and Vikram Vishal*

Cite This: *ACS Omega* 2025, 10, 4395−4405

Read Online

ACCESS | Metrics & More | Article Recommendations

ABSTRACT: Shale reservoirs, often acting as caprocks for conventional hydrocarbon reservoirs, exhibit moderate to high porosity and remarkably low permeability. Organic-rich shales serve as reservoirs for unconventional hydrocarbons. This study focused on evaluating the characteristics of the source rocks and the factors influencing pore parameters in organic-rich shale from a Permian Basin in India, exploring its feasibility as both a CO_2 sink and a natural gas source. Experimental techniques were employed to explore the mineral and the organic matter characteristics along with attributes of the pores hosted within them. The investigated shales displayed diverse thermal maturity levels, spanning from that in oil-prone to gas-prone zones, with the total organic carbon content varying from 0.72 to 24.98 wt %, indicating substantial organic richness. Rock-Eval pyrolysis results revealed a range of thermal maturity (T_{max}) values between 426 and 474 °C, while X-ray diffraction analysis indicated significant quantities of illite and kaolinite, along with trace amounts of pyrite in certain samples. Field-emission scanning electron microscopy imaging and its detailed interpretation provided valuable insights into the pore structure and arrangement. In our study, we found that both the clay content and the organic matter significantly contribute to gas adsorption. While clay content strongly influences mesopore attributes, the organic matter predominantly affects micropore attributes. Furthermore, a direct relationship among fractal dimension, surface area, and pore volume, indicating increased complexities with these variables. Our examination of mesopore fractal attributes revealed that smaller mesopores exhibit a more convoluted and irregular configuration in comparison to the larger ones. These findings provide significant insights into the pore morphology of the analyzed shale sample.



Downloaded via TU DELFT on February 11, 2025 at 13:48:49 (UTC).
See https://pubs.acs.org/sharingguidelines for options on how to legitimately share published articles.

1. INTRODUCTION

Understanding pore morphology, sorption properties, and gas storage capacities within organic-rich shale formations is crucial due to the potential significant reserves of trapped gas.[1] Traditionally, shale formations are commonly seen as impermeable barriers or cap rocks. However, progress in drilling methods and hydraulic fracturing has facilitated the extraction of gas confined within shale matrix.[2] In addition, in situ thermal stimulation of shale enhances hydrocarbon mobility and release, especially in low-permeability formations, thereby improving extraction efficiency.[3−5] Shale formations containing high organic matter act as both source and reservoir rocks, owing to their organic content and intricate pore matrix, facilitating gas generation, transport and storage.[6] Complexities within the shale formations arise from the variability in depositional conditions and the blending of organic and inorganic constituents, necessitating scientific analysis.[7,8] Most of the gas in shale is stored via adsorption on pore surfaces,[9−12] with pores classified as macro-, meso-, or nanopores based on their size, each impacting gas transport and storage differently.[13] Recently, CO_2-enhanced shale gas production has emerged as a method for the extraction of gas while also enabling CO_2 storage in depleted reservoir.[14] Shale pore characteristics—such as porosity, pore volume, specific surface area, and connectivity—significantly influence the storage and transport potential of both methane and CO_2, making their accurate characterization crucial for reserve estimation, production forecasting, and CO_2 sequestration planning.[15,16]

Given the inherent complexity and variability, extensive research is essential to understand the pore network in shale formations.[6,8,17] Organic content plays a crucial part in gas storage and production by contributing to the internal surface area as well as controlling the heterogeneity and anisotropy of the shale matrix.[18−20] Parameters such as thermal maturity,

Received: August 6, 2024
Revised: December 6, 2024
Accepted: December 13, 2024
Published: February 2, 2025



© 2025 The Authors. Published by American Chemical Society

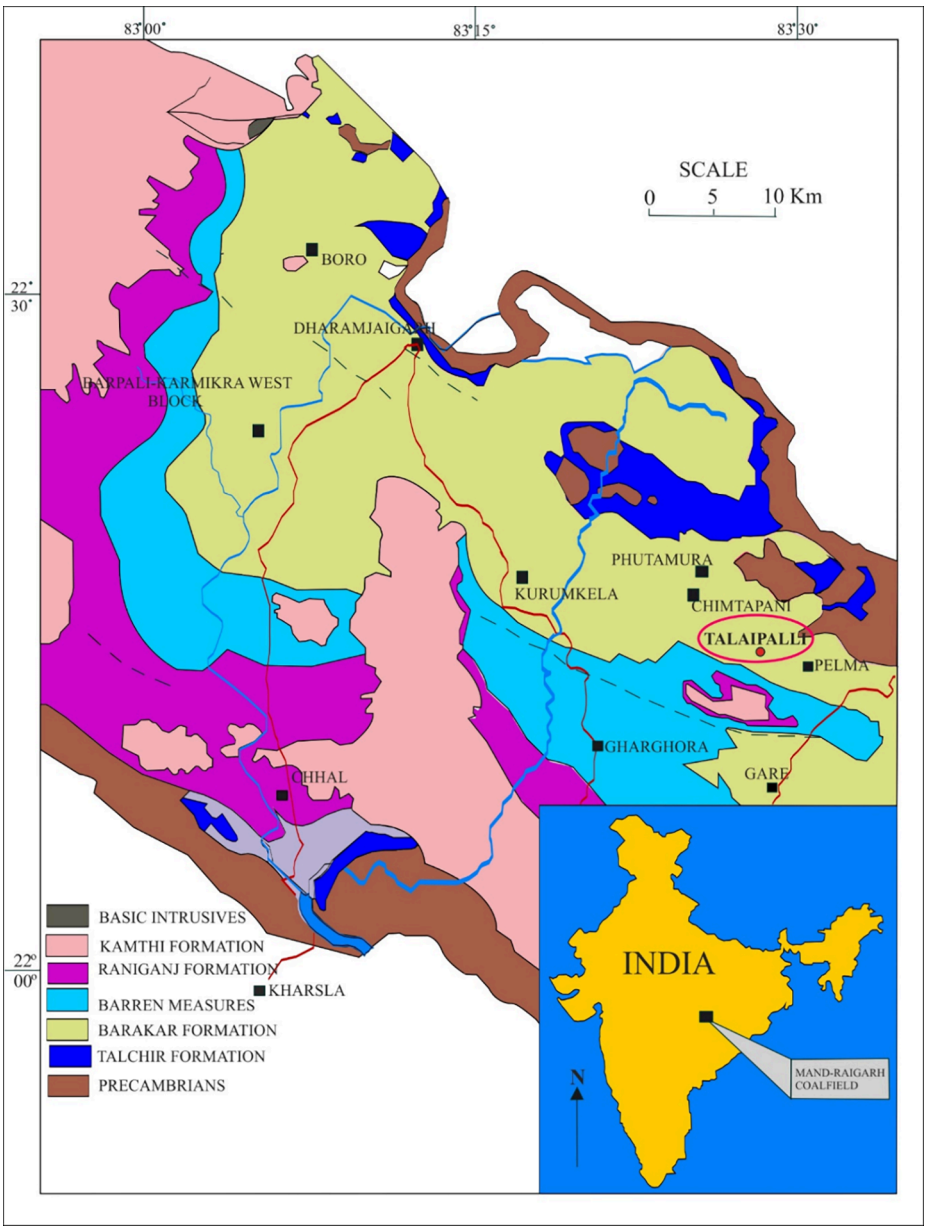


Figure 1. A geological map of the Mand-Raigarh basin is presented, indicating the location of the study area.[47] Figure reproduced with permission from American Chemical Society, copyright 2023.

mineral composition, kerogen types, and total organic carbon influence gas production and storage within the shale reservoirs.[8,21−24] Many studies have also experimentally illustrated how changes in temperature and treatment conditions alter pore structural properties in shales.[25−27]

Various methods, such as microscopy and gas adsorption techniques, are employed to investigate the attributes of pore structure, offering insights into pore size distribution in shale.[28−34] These methods offer detailed observations of the pore geometry, size, volume, surface area, and width, contributing to a comprehensive understanding of shale pore systems. Mandelbrot[35] introduced the concept of the fractal dimension (D_s) to assess surface pore irregularity and roughness in porous media. This theory has been applied to determine surface roughness in shales using N_2 adsorption isothermal curves, as evidenced by several studies.[22,36−39] The roughness of pore surfaces plays a crucial role in oil and gas flow within shale reservoirs, underscoring the significance of fractal dimension in characterizing the shale pore structure. Fractal models such as the Frenkel−Halsey−Hill (FHH) equations have been employed to analyze surface irregularities of solid surfaces using the adsorption isotherm.[37−40] The goal of this study is to analyze the pore characteristics of shales from the Mand-Raigarh basin, Chhattisgarh. To enhance our understanding of the morphology of pores and delineate the impact of mineral composition and total organic carbon (TOC) content on the properties of shale gas reservoirs, we employed various techniques including X-ray diffraction (XRD) analysis, field-emission scanning electron microscopy (FE-SEM) imaging, and low-pressure N_2 and CO_2 adsorption. These methods helped us characterize the pore structures, pore size distribution, specific surface area (SSA), and total pore volume (TPV) of shale cores. We examined how mineral composition and TOC content influence pore structure and

https://doi.org/10.1021/acsomega.4c07214
ACS Omega 2025, 10, 4395−4405

Table 1. Mand-Raigarh Basin's Lithostratigraphic Succession in India[47]

geologic age	formation	lithology
recent to subrecent	Upper Kamthi	alluvium and laterite
Upper Permian to Jurassic	Lower Kamthi	fine- to medium-grained sandstone, carbonaceous shale, and coal bands with greenish sandstone
unconformity		
Upper Permian	Raniganj	fine- to coarse-grained sandstone, gray and carbonaceous shales, persistent coal seams
Middle Permian	Barren Measures	fine to coarse medium-grained sandstone, grayish to carbonaceous shales
Lower Permian	Barakar	coarse- to fine-grained sandstone, shales, carbonaceous shales, coal seams
	Karharbari	medium- to coarse-grained white arkosic sandstone, carbonaceous shales and coal seams
Upper Carboniferous to Lower Permian	Talchir	dimictite, green shale, rhythmites, and sandstone
unconformity		
Precambrian	unclassified Precambrian rocks	gneisses, schists, pegmatite, etc.

Table reproduced with permission from American Chemical Society, copyright 2023.

used the FHH theory[41] to investigate the fractal dimensions derived from N_2 adsorption data to estimate the heterogeneity of the pore surface and structure. The findings provide valuable insights into the distribution of the pore structure and its influencing factors on shale gas adsorption, aiding in the exploration of shale gas potential in the study region.

Several studies have examined the pore characterization of Indian shales, highlighting their gas storage potential.[9,42,43] However, the pore attributes of the Mand-Raigarh basin in Central India remain unexplored. Understanding these characteristics will provide valuable insights into shale gas storage and exploration, alongside opening avenues for CO_2 sequestration.[44,45] This alternative could reduce the nation's dependence on conventional energy sources.

2. STUDY AREA

India's Mand-Raigarh basin, which spans an area of more than 900 km^2, is located within the Mahanadi Basin and is bordered by 21°45′00″ and 22°42′00″ latitudes and 83°01′00″ and 83°44′00″ longitudes.[46] The Talaipalli Coal Mine is situated close to Talaipalli village in the Gahrghoda block of Raigarh district, Chhattisgarh, India, at latitude 22°14′26″N and longitude 83°27′39″E. It is located about 55 km from Raigarh town and has a 21.13 km^2 area. The Talaipalli coal block is located in the eastern half of the Mand-Raigarh coalfield and predominantly relies on the Barakar Formation's coal-bearing sedimentary layers, with Barren Measure coal strata dominating the block's southern region. Shale strata with varying lateral thicknesses make up the Lower Permian Barakar Formation in the basin. Figure 1 displays a geological map, indicating the positions of the test borehole drilled in shale formations. Table 1 provides an overview of the lithology and associated geological ages, illustrating a comprehensive stratigraphic sequence.

3. SAMPLING AND METHODOLOGY

The research work was carried out on five variety of specimens belonging to the Barakar Formation. These shale samples were sourced from depths ranging between 345 and 886 m (Table 2). The nomenclature included a "MR" prefix followed by sequential numbers, such as MR1 for the sample obtained from 345 m and MR5 for the one collected from 886 m. To preserve the integrity of the cores, they were sealed in labeled bags and brought to the lab. For further analysis, a portion of each core was sectioned into flat chips (5 × 10 × 10 mm) for FE-SEM

Table 2. Shale Samples and Their Depths

sample ID	depth (m)
MR1	345
MR2	513
MR3	610
MR4	776
MR5	886

imaging, while the remaining material was crushed and passed through a 212 μm (72 mesh) sieve. The sieved fraction were used for XRD, Rock-Eval pyrolysis, and low-pressure gas adsorption (LPGA) analyses, with each technique described in the following subsections.

3.1. X-ray Diffraction Studies. Mineral and organic components stand out as the most critical parameters in understanding shale's origins and diagenetic processes. XRD analysis was carried out to quantify mineralogy of the shales using a PANalytical's X'Pert Pro system equipped with a Cu anode. In this analysis, 5 mg of the sieved shale powder fraction was utilized. The scanning was conducted with a step size of 0.0130°/s and covered a 2θ range from 5 to 70°. Rietveld refinement was followed to identify the mineral peaks.[48] Highscore X'Pert Pro software was employed to evaluate the relative mineral abundance.

3.2. High-Resolution Imaging. FE-SEM visualizes and identifies pores and organic matter at nanometer scales. In this study, FE-SEM equipment was utilized for SEM, enabling imaging at magnifications up to 450,000× with a maximum operating voltage of 30 kV. To enhance surface conductivity, chip samples were sputter-coated with gold before imaging. Various magnifications were employed to identify pores of varied sizes.

3.3. Rock-Eval Pyrolysis. The Rock-Eval 6 analyzer was utilized to evaluate the source-rock potential of the shale samples. To analyze the shales, we followed a revised protocols for accurate estimation of TOC.[7,49,50] To study the characterization of potential source rock, 5−10 mg of samples was used in the analysis. Initially, the crucibles filled with powdered shales were inserted into the pyrolysis chamber and exposed to isothermal heating at 300 °C. During this process, hydrocarbons released were carried by N_2 and detected using a flame ionization detector (FID), represented by the "S_1" peak. Subsequently, the shales were heated from 300 to 650 °C at a rate of 25 °C/min, causing the decomposition of organic matter into hydrocarbon. These hydrocarbons, also trans-

https://doi.org/10.1021/acsomega.4c07214
ACS Omega 2025, 10, 4395−4405

ported by N_2, were detected by the flame ionization detector (FID) and is identified as the "S_2" peak. The T_{max}, indicates the temperature at which peak hydrocarbon generation during the S_2 stage was recorded, aiding in the assessment of organic matter thermal maturity within the shale samples. Additionally, oxygenated compounds within the organic matter decomposed during the pyrolysis stage, yielding CO_2 and CO, detected as the "S_3" peak. The carbon generated during stages S_1, S_2, and S_3 collectively contributed to the pyrolyzable carbon (PC) fraction. Following the pyrolysis phase, the samples were heated within the oxidation chamber. This process provided data on the quantity of residual carbon (RC) present in the shale samples. The sum of both the PC and RC fractions gives the total organic carbon (TOC) . Furthermore, empirical formulas were applied to determine additional indices, specifically, the hydrogen index (HI) and oxygen index (OI).

$$\text{hydrogen index (HI)} = [(S_2/\text{TOC}) \times 100] \quad (1)$$

$$\text{oxygen index (OI)} = [(S_3/\text{TOC}) \times 100] \quad (2)$$

3.4. Low-Pressure Gas Adsorption (LPGA). To examine the studied shale samples, N_2 and CO_2 gases were used as probing agents to explore the mesopores and micropores, respectively. A quantity of 2−3 g of powdered shale underwent degassing under a pressure of 10^{-4} Torr for 12 h at 110 °C[12,51−53] to remove moisture and volatiles present within the pores of shale samples. Chandra et al.[25] emphasized the importance of selecting an appropriate degassing temperature to minimize errors in determining pore attributes. Research has shown that a degassing temperature of 110 °C effectively removes moisture and lowers hydrocarbons without altering shale pores.[52,53] Research conducted by Singh et al.[54] and Chandra et al.[25] has demonstrated that raising the degassing temperature from 110 to 200 °C and 300 °C leads to changes in pore attributes due to the breakdown of organic matter. Some researchers have used a degassing temperature of 250 °C,[36] noting a minimal mass change (approximately 1−2%) in solid organic matter, but this approach is less effective for shales with lower thermal maturity. To maintain consistency, 110 °C is widely accepted as it causes a minimal mass change in solid organic matter.

Quantachrome Autosorb iQ physisorption analyzer was used to carry out the adsorption studies. It gives us information about the quantity of gas adsorbed or desorbed at specific pressure levels. N_2 molecules, characterized by their quadrupolar and non-reactive nature, exhibit preferential adsorption within selective functional groups. This characteristic renders N_2 highly suitable as a probe gas for conducting physisorption experiments. Adsorption of N_2 at a temperature of 77 K aligns with the point at which pure N_2 condenses at standard temperature and pressure. The examination of adsorption and desorption behaviors extends over a spectrum of relative pressures (P/P_0) ranging from 0.001 to 0.99. In this case, P is the pressure of probe gas and P_0 represents the condensation pressure of liquid N_2 at 77 K (760 Torr). The desorption branch of the isotherm is obtained by reversing the adsorption process, during which the liquid adsorbate is released, resulting in a decrease in the equilibrium relative pressure. The notable hysteresis loop generated by adsorption and desorption isotherms, which remain consistent across consecutive cycles, emphasizes the importance of understanding hysteresis behaviors. Such comprehension is vital for effectively tackling practical challenges characterizing pore structures. Despite its limitations in probing micropores smaller than 1.3 nm, N_2 was chosen for adsorption measurements due to its ability to bind to specific activation sites and effectively explore pores larger than 1.3 nm in diameter. The N_2 adsorption model was applied to obtain various parameters including the Brunauer−Emmett−Teller (BET) surface area and pore size distribution (PSD) determined through density functional theory (DFT). Additionally, the fractal dimension of mesopores was calculated using the FHH method.

CO_2 adsorption was carried out at a temperature of 273 K using a water bath, examining relative pressures between 0.0005 and 0.03, with P_0 fixed at 26,610 Torr. CO_2 was chosen as the adsorbate for micropore characterization due to its strong affinity for organic carbon, allowing it to penetrate shale micropores. This process calculates the Dubinin−Radushkevich (D-R) surface area, Dubinin−Astakhov pore volume, and PSD for the CO_2 adsorption. The CO_2 adsorption isotherms were analyzed by using the DFT method. In summary, the integration of N_2 and CO_2 adsorption methods allowed for a thorough investigation of the pore properties. This comprehensive analysis provided valuable information about the structure of the pores of the shale samples.

4. RESULTS

The experimental procedures were used to evaluate the pore characteristics and the PSD, and how they affect the effective surface area of the shale samples. Mineral and organic matter quantification, LPGA measurements, and FE-SEM analyses were done to characterize and illustrate various categories of pores, as elaborated in this section.

4.1. Mineral Composition. The mineral content of the samples was examined using XRD analysis, with the results presented in Figure 2. Quartz and clay minerals constitute the primary mineral components, with illite being the dominant clay mineral, ranging from 16 to 49%. It is worth noting that illite-rich shale exhibits a significant volume of micropores.[55] Among the samples, MR5 exhibits the highest quartz content, while MR3 shows the lowest one. Conversely, MR3 has the highest clay content, while MR5 has the lowest one. Feldspar is identified in MR1, MR3, and MR4, while it is absent in MR2 and MR5. Pyrite, as a heavy mineral, is present in MR2 only among the examined shale samples.

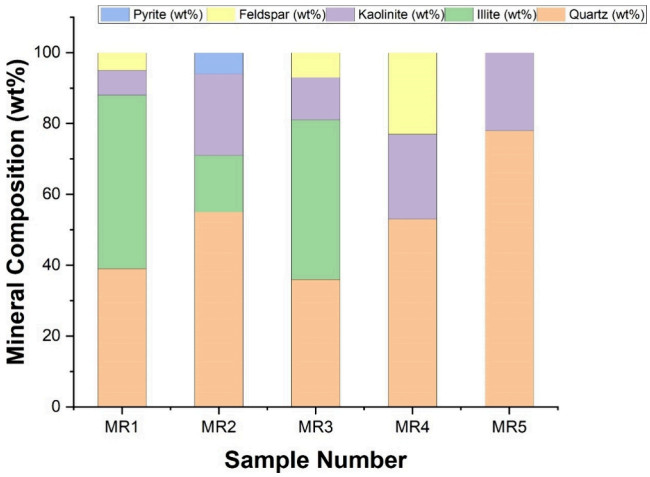


Figure 2. Mineral composition of the studied shale samples from Mand-Raigarh.

https://doi.org/10.1021/acsomega.4c07214
ACS Omega 2025, 10, 4395−4405

Table 3. Rock-Eval Results of the Studied Shale Samples

sample number	depth (m)	S_1 (mg/g)	S_2 (mg/g)	S_3 (mg/g)	T_{max} (°C)	TOC (%)	HI (mg HC/g TOC)	OI (mg CO_2/g TOC)	$S_1 + S_2$ (mg/g)
MR1	345	0.42	82.17	2.08	426	24.98	329	8	82.59
MR2	513	0.35	63	0.69	431	13.97	451	5	63.35
MR3	610	0.17	24.74	0.66	431	13.07	189	5	24.91
MR4	776	0.01	0.29	0.08	454	0.72	40	11	0.30
MR5	886	0.08	2.04	0.31	474	5.7	36	5	2.12

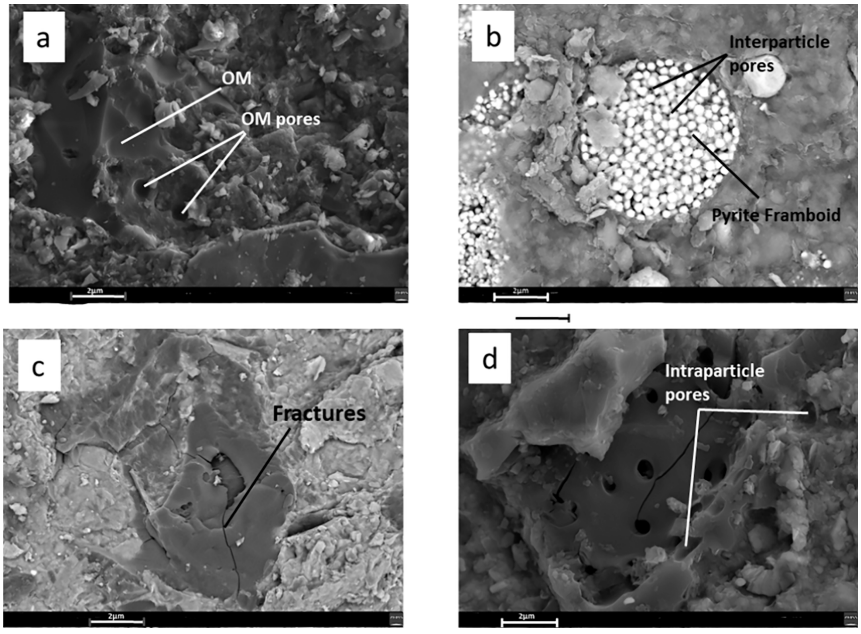


Figure 3. FE-SEM images illustrating various types of pores in shale samples. (a) Macropores in organic matter, (b) interparticle pores in pyrite framboid, (c) natural fractures in shale samples, and (d) intraparticle pores in quartz and OM pores.

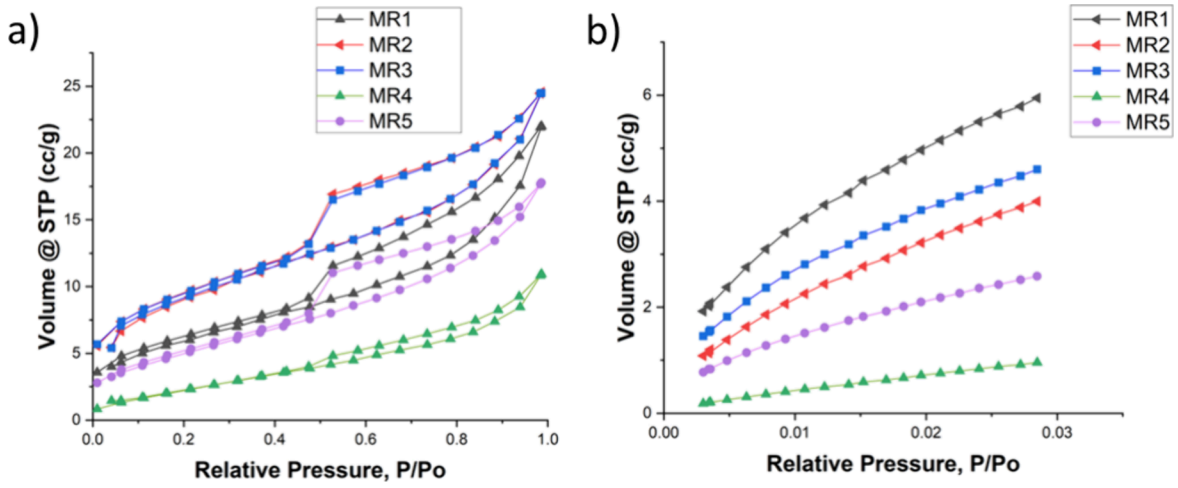


Figure 4. (a) Low-pressure N_2 adsorption isotherm and (b) low-pressure CO_2 adsorption isotherm of the studied shales.

4.2. Thermal Maturity and Organic Content. The Rock-Eval experiment results for the shale samples are outlined in Table 3. S_1 and S_2 values are combined to give the genetic potential (GP). T_{max} shows different thermal levels within the studied samples. MR1, MR2, and MR3 show "immature" thermal maturity, MR4 demonstrate a "late mature" level, and MR5 represents a "postmature" condition.[56] The HI is a metric for evaluating the type of kerogen present and the thermal maturity level of organic materials.[57] The HI and OI of the studied samples range between 36 and 451 mg HC/g of TOC and 5 and 11 mg CO_2/g of TOC, respectively. These findings suggest that the majority of the samples fall under the kerogen types II and III and type III. The GP of source rocks is characterized as follows: values ranging from 2 to 5 signify low production potential, those falling between 5 and 10 are deemed moderate, and values surpassing 10 suggest high to very strong production potential.[58] The analyzed samples demonstrate a genetic potential (GP) ranging from 0.30 to 82.59 mg/g, representing a spectrum from poor to exceptional source potential for the source rocks (Table 3).

https://doi.org/10.1021/acsomega.4c07214
ACS Omega 2025, 10, 4395−4405

Table 4. Meso- and Micropore Attributes of the Shale Samples

	specific surface area (SSA) (m^2/g)		average pore width (nm)		total pore volume (TPV) (cc/g)		
sample ID	micropore	mesopore	micropore	mesopore	micropore	mesopore	micro + meso
MR1	65.51	21.58	0.882	6.309	0.025	0.034	0.059
MR2	48.85	31.79	0.956	4.779	0.018	0.037	0.055
MR3	50.85	31.96	0.890	4.744	0.019	0.038	0.057
MR4	14.06	9.69	1.072	6.984	0.005	0.016	0.021
MR5	28.71	18.97	0.904	5.801	0.011	0.028	0.039

4.3. Morphology of Pores. The representative images are provided to illustrate various pore types present within the shale samples (Figure 3). In these images, empty pores are depicted as black, while those filled with organic matter appear gray, and mineral-filled pores are portrayed as bright. Loucks et al.[30] proposed a classification for matrix-related pores, dividing them into three primary types: (i) organic matter (OM) pores (Figure 3a), (ii) interparticle pores, found between mineral particles (intergranular) (Figure 3b), and (iii) intraparticle pores, present within mineral particles (intragranular) (Figure 3d). These types are all observed in the studied samples. Additionally, natural fractures, visible under an electron microscope, display various forms, primarily at the micrometer scale, and are often observed within quartz grains or OM−clay aggregates (Figure 3c).

4.4. Characteristics of Pores. Figure 4 shows the sorption isotherms of the shale samples. The low-pressure N_2 adsorption profile of the shale samples (Figure 4a) exhibited typical features of type IV adsorption and H3 hysteresis according to IUPAC classification standards. The presence of hysteresis suggests the existence of mesopores and macropores within our shale samples. The H3 hysteresis pattern observed indicates the influence of tensile strength on the samples, likely owing to the presence of cavitation and ink-bottle pores.[59] Notably, among all of the samples, MR3 exhibited the highest adsorption potential at 24.57 cc/g, while MR4 demonstrated the lowest one at 10.94 cc/g.

The micropore attributes of the samples were assessed through CO_2 adsorption (Figure 4b). The observed isotherms exhibit characteristic features of type II, with a notable increase in the P/P_0 range from 0.0005 to 0.01. Among the analyzed shale samples, MR1 demonstrated the highest CO_2 adsorption potential at 5.95 cc/g, while MR4 displayed the lowest potential at 0.95 cc/g. This suggests that MR1 has a greater extent of micropore filling, while MR4 has the least.

4.4.1. Pore Attributes. The mesopore characteristics are studied using N_2 gas adsorption, while the micropore properties are examined using CO_2 gas adsorption. The mesopore surface area is evaluated using the BET equation. From the N_2 adsorption isotherm analysis, it was found that sample MR3 had the maximum BET surface area of 31.96 m^2/g, whereas sample MR4 exhibited the lowest value of 9.69 m^2/g (Table 4). To analyze PSD for CO_2 and N_2 adsorption, the adsorption curves are scrutinized using CO_2 DFT and quenched solid DFT models, respectively. The TPV is determined by combining the values of meso- and micropore volume. Among the samples, MR1 demonstrates the highest pore volume at 0.059 cc/g, while MR4 exhibits the lowest pore volume at 0.021 cc/g. Additionally, MR4 demonstrates the highest average pore width of 6.98 nm, compared to MR3, which has the smallest average pore width of 4.74 nm.

4.4.2. Pore Size Distribution (PSD). The PSD curves depict how the pore volume is distributed relative to the pore size. In these curves, those derived from CO_2 adsorption end at 2 nm, while those from N_2 adsorption commence at 2 nm, indicating a smooth transition between the two. Consequently, merging these PSD curves into a single curve (Figure 5) provides

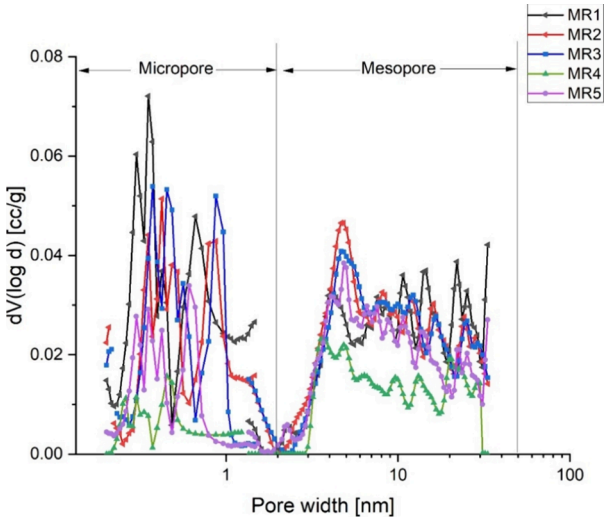


Figure 5. Combined CO_2 and N_2 DFT plot of the shale samples showing pore size distribution.

comprehensive insight into the pore structure of shale. In the CO_2 PSD, each shale sample shows a multimodal distribution characterized by noticeable peaks typically ranging from 0.4 to 0.9 nm. MR1 displays the highest peak around 0.5 nm, consistent with those of other samples. On the other hand, the N_2 PSD reveals distinct sharp peaks between 4 and 30 nm for all samples. MR2 exhibits the highest peak within this range, similar to those of the other shale samples.

4.4.3. Fractal Dimension. Fractal dimension (D_s) was proposed by Mandelbrot to characterize surface roughness. With an increase in surface roughness, D_s increases. The range varies between 2 and 3, with 2 indicating a perfectly smooth surface and 3 indicating a highly rough surface. Regardless of the scale, fractal surfaces exhibit a recurring pattern of irregularities, as first described by Avnir et al.[60] The FHH theory[61] is utilized in the formulation of the multilayer adsorptive model. The expression for this model is as follows:

$$\ln(V/V_m) = C + A\ln[\ln(P/P_0)] \quad (3)$$

In the formula, V represents the volume of N_2 adsorbed at equilibrium pressure P, the gas volume in the monolayer is denoted by V_m, P_0 is the saturation pressure of N_2 at 77 K, C is a constant, and A is the power-law exponent that depends on D_s. The interaction between the adsorbent and the adsorbate is mainly controlled by van der Waals forces due to the very low surface tension at extremely low relative pressures. This results

https://doi.org/10.1021/acsomega.4c07214
ACS Omega 2025, 10, 4395−4405

in a well-established correlation between A and D_s, formulated as follows:

$$A = D_s - 3 \quad (4)$$

Capillary condensation becomes more significant at elevated P/P_0 ratios as the surface tension rises, causing a modification in eq 2 to

$$A = (D_s - 3)/3 \quad (5)$$

The fractal dimension, which is studied from the N_2 adsorption isotherm, is categorized into two segments. The initial segment, where the P/P_0 ranges between 0.01 and 0.5, is denoted as D_1, while the subsequent portion, where P/P_0 ranges between 0.5 and 0.99, is represented as D_2. In the low-pressure regime, the primary interaction between the solid surface and the gas interface is dictated by the prevailing van der Waals force of attraction. This interaction results in the fluid interface mirroring the surface roughness, leading to the computation of D_s using eq 4 in this context. Conversely, in the high-pressure regime, the interaction between the solid and gas phases is predominantly influenced by surface tension and capillary condensation. Here, the gas interface moves away from the solid surface, causing a reduction in the interface area, and subsequently, the D_s has been determined using eq 5. The FHH approach was employed for the analyzed shale samples, with detailed information on the fractal dimension calculations provided in Table 5.

Table 5. Fractal Dimension of the Shale Samples Assessed across Varying Ranges of Relative Pressure

sample number	$D_1(3 + S_1)$ $(0.01 < P/P_0 < 0.5)$	R_1^2	$D_2(3 + 3S_2)$ $(0.5 < P/P_0 < 0.99)$	R_2^2
MR1	2.48	0.99	2.11	0.99
MR2	2.51	0.99	2.35	0.99
MR3	2.57	0.99	2.34	0.99
MR4	2.20	0.97	2.08	0.99
MR5	2.41	0.98	2.17	0.99

5. DISCUSSION

Based on the data obtained from the experiments, it has been observed that sample MR1 exhibited the highest computed D-R surface area, while MR4 displayed the lowest one, reflecting a similar trend observed in the DA total pore volume. The PSD determined from the combined CO_2–N_2 curve depicted multimodal peaks for the analyzed samples. In N_2 DFT, the highest peak is shown by MR2 around 4 nm, whereas in CO_2 DFT, the highest peak is shown by MR1 around 0.5 nm.

MR1 exhibits a higher micropore SSA, potentially attributed to its elevated organic content. Conversely, MR4, with the lowest organic content, tends to display a lower micropore SSA. This suggests a notable relation between the composition of organic matter and the attributes of microporosity. Furthermore, the MR3 sample, characterized by the highest clay content, contributes the highest BET SSA.

Figure 6 illustrates that the clay mineral and TOC content display a positive correlation with pore parameters, indicating their primary role in pore formation. Specifically, Figure 6a shows that clay minerals correlate more strongly with mesopore volume than with TOC. Conversely, Figure 6c reveals a stronger correlation between TOC and micropore volume compared to clay minerals. In Figure 6b, clay minerals contribute significantly to achieving a good fit with the mesopore surface area, whereas the TOC content results in a weaker fit for this parameter. However, the D-R micropore surface area derived from CO_2 adsorption demonstrates an excellent fit with the TOC content, in contrast to a lower fit with clay content (Figure 6d). TOC content and micropore parameters align with patterns commonly suggested in earlier research.[31,62,63]

This suggests that while clay minerals have a greater influence in the mesopore region, the TOC content plays a more significant role in the micropore region. Considering the significant roles of clay minerals and organic carbon in adsorption, our results indicate that both clay minerals and organic matter have a major impact on gas adsorption. This challenges the traditional notion that gas adsorption in shale is governed primarily by organic matter alone. Instead, our results suggest that clay minerals also play a significant role in adsorption, thereby enhancing the gas storage capacity.

Figure 7 illustrates how the fractal dimensions of shale pores are influenced by primary minerals and TOC. The correlation between D_1 and D_2 with clay mineral content (Figure 7a) exhibits a stronger influence than that with TOC (Figure 7c), indicating the predominance of smaller mesopores associated with clay minerals. In contrast, the values of D_1 and D_2 show no clear trend with increasing quartz content (Figure 7b), suggesting that quartz has a negligible effect on the pore surface and structure.

Figure 8 illustrates the correlations between pore attributes and fractal dimensions (D_1 and D_2). In Figure 8a, the mesopore volume demonstrates an excellent fitting in the low-pressure regime (D_1) and a good fitting in the high-pressure regime (D_2). The fractal parameters D_1 and D_2 exhibit notable significance concerning mesoporous SSA (Figure 8b). The BET surface area has a stronger correlation with the fractal dimension D_1 than with D_2, suggesting that smaller mesopores have a greater influence on the BET surface area and pore volume. A negative correlation exists between fractal dimension and average pore diameter (Figure 8c). The average pore diameter decreases as the fractal dimension increases. Shales with smaller average pore diameters generally exhibit a higher number of mesopores and a more complex pore structure.

Numerous researchers have identified comparable correlations and fitted curves, assessing their accuracy with the coefficient of determination (R^2). Similar correlations between fractal dimensions and organic matter, mineral content, and pore parameters were noted by Li et al.[64] They found a positive relationship with mesopore SSA and a negative relationship with average pore width. The study highlighted that the clay mineral content has a stronger influence compared with organic matter in shale samples. Similarly, Xu et al.[65] demonstrated correlations between pore structure parameters, TOC, and mineral content. Their study revealed a significant relationship with the total organic content, with a minimal correlation with mineral matter. Xu et al.[65] noted a relationship between pore structure attributes and mineral content, indicating a positive correlation with TOC and a negative correlation with clay. Given the consistency of the correlations observed in our study with other global examples, we have confidence in the validity of these associations within our experimental constraints.

https://doi.org/10.1021/acsomega.4c07214
ACS Omega 2025, 10, 4395−4405

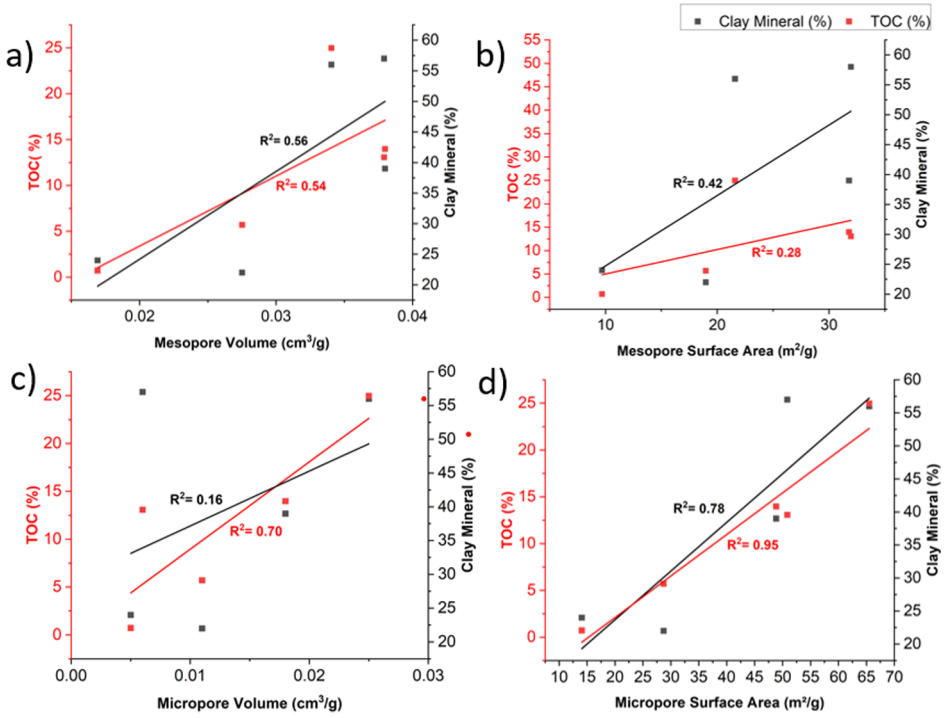


Figure 6. Correlation of (a) mesopore volume with TOC and clay mineral, (b) mesopore surface area with TOC and clay mineral, (c) micropore volume with TOC and clay mineral, and (d) micropore surface area with TOC and clay mineral.

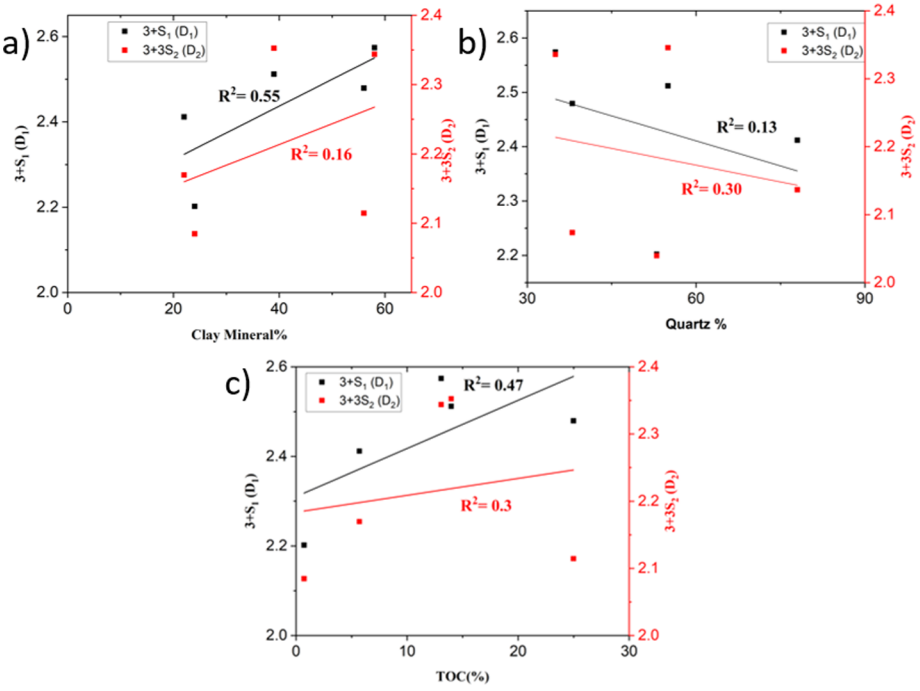


Figure 7. Relationships between fractal dimensions and (a) clay content, (b) quartz, and (c) TOC depicted in the diagram.

6. CONCLUSIONS

This research aimed to assess the gas storage capacity of shale samples from the Mand-Raigarh basin and explore the relationship between pore attributes and mineral/organic matter content. The primary findings of this investigation are outlined below.

1. TOC and clay minerals are the primary contributors to shale porosity. The micropore SSA ranges from 14.06 to 65.51 m^2/g, while the mesopore SSA spans 9.69−21.58 m^2/g, with the total pore volume varying from 0.021 to 0.059 cm^3/g. Notably, mesopore parameters correlate more strongly with clay content, while micropore parameters align well with the organic carbon content, explaining the influence of both on gas storage in shale formations.
2. N_2 gas adsorption analysis shows that mesopores dominate the shale samples, comprising 57.63−76.19%

https://doi.org/10.1021/acsomega.4c07214
ACS Omega 2025, 10, 4395−4405

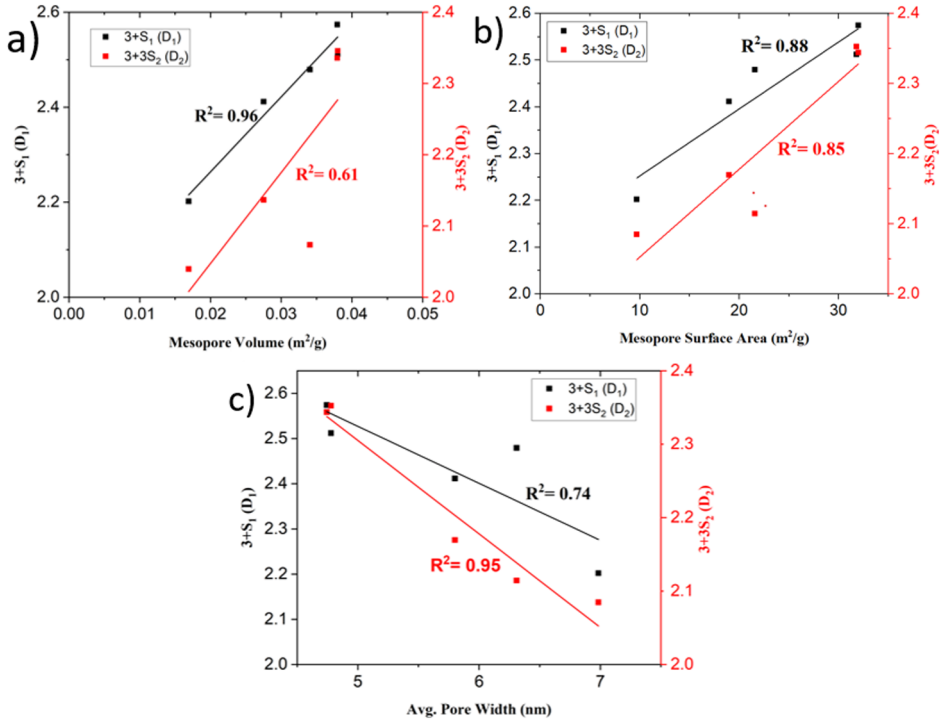


Figure 8. Relationship between fractal dimension and (a) mesopore volume, (b) mesopore SSA, and (c) average pore width.

of the pore volume, while CO_2 gas adsorption reveals that micropores account for 23.81−42.37%. Among the samples, MR3 has the highest mesopore volume, and MR1 has the highest micropore volume.

3. The fractal characteristics of mesopores indicate that smaller mesopores have rougher surface textures, while larger ones are smoother, as reflected in the average fractal dimensions (D_1 = 2.43 and D_2 = 2.21). Additionally, the fractal dimension rises with increased BET SSA and mesopore volume but decreases with larger average pore widths, suggesting that narrower mesopores have a more complex structure that may enhance gas adsorption.

AUTHOR INFORMATION

Corresponding Author

Vikram Vishal − *Computational and Experimental Geomechanics Laboratory, Department of Earth Sciences, National Centre of Excellence in Carbon Capture, Utilization and Storage, and Interdisciplinary Programme in Climate Studies, Indian Institute of Technology Bombay, Mumbai 400076, India;* orcid.org/0000-0002-0896-7844; Phone: +91-22-2576-7254; Email: v.vishal@iitb.ac.in

Authors

Saheli Ghosh Dastidar − *Department of Applied Geology, Indian Institute of Technology (ISM) Dhanbad, Dhanbad 826004, India*

Kripamoy Sarkar − *Department of Applied Geology, Indian Institute of Technology (ISM) Dhanbad, Dhanbad 826004, India*

Debanjan Chandra − *Department of Geoscience and Engineering, Delft University of Technology, Delft 2628 CN, The Netherlands*

Bodhisatwa Hazra − *CSIR−Central Institute of Mining and Fuel Research, Dhanbad 826015, India;* orcid.org/0000-0002-3462-7552

Complete contact information is available at: https://pubs.acs.org/10.1021/acsomega.4c07214

Notes

The authors declare no competing financial interest.

ACKNOWLEDGMENTS

The authors gratefully acknowledge IIT (ISM) Dhanbad, and IIT Bombay for providing the necessary laboratory facilities to conduct the research works. No additional funding was received by any of the authors to complete this work.

ABBREVIATIONS

P: vapor pressure (in Torr)
P_0: condensation pressure of nitrogen at 77 K (in Torr)
V: nitrogen adsorption volume on the adsorbent at equilibrium pressure (P/P_0) (in cc)
V_m: volume of gas at monolayer adsorption (in cc)
A: power-law exponent depending on D_s
T_{max}: thermal maturity
PC: pyrolyzable carbon
RC: residual carbon
TOC: total organic carbon
HI: hydrogen index
OI: oxygen index

REFERENCES

(1) Ross, D. J. K.; Marc Bustin, R. The importance of shale composition and pore structure upon gas storage potential of shale gas reservoirs. *Mar. Pet. Geol.* **2009**, *26*, 916−927.

(2) Middleton, R. S.; Gupta, R.; Hyman, J. D.; Viswanathan, H. S. The shale gas revolution: Barriers, sustainability, and emerging opportunities. *Appl. Energy.* **2017**, *199*, 88−95.
(3) Hazra, B.; Chandra, D.; Vishal, V.; Ostadhassan, M.; Sethi, C.; Saikia, B. K.; Pandey, J. K.; Varma, A. K. Experimental study on pore structure evolution of thermally treated shales: implications for CO2 storage in underground thermally treated shale horizons. *Int. J. Coal Sci. Technol.* **2024**, *11* (1), 61.
(4) Krumm, R. L.. *Carbon dioxide sequestration in in situ thermally treated coal and oil shale formations*. The University of Utah; 2014.
(5) Kelly, K. E.; Wang, D.; Hradisky, M.; Silcox, G. D.; Smith, P. J.; Eddings, E. G.; Pershing, D. W. Underground coal thermal treatment as a potential low-carbon energy source. *Fuel Process. Technol.* **2016**, *144*, 8−19.
(6) Ross, D. J.; Bustin, R. M. Shale gas potential of the lower Jurassic Gordondale member, northeastern British Columbia, Canada. *Bull. Can. Pet. Geol.* **2007**, *55* (1), 51−75.
(7) Hazra, B.; Karacan, C.Ö.; Tiwari, D. M.; Singh, P. K.; Singh, A. K. Insights from Rock-Eval Analysis on the Influence of Sample Weight on Hydrocarbon Generation from Lower Permian Organic Matter Rich Rocks, West Bokaro Basin. *India. Mar. Pet. Geol.* **2019**, *106*, 160−170.
(8) Chandra, D.; Vishal, V.; Debbarma, A.; Banerjee, S.; Pradhan, S. P.; Mishra, M. K. Role of Composition and Depth on Pore Attributes of Barakar Formation Gas Shales of Ib Valley, India, Using a Combination of Low-Pressure Sorption and Image Analysis. *Energy Fuels* **2020**, *34*, 8085.
(9) Chandra, D.; Vishal, V. A comparison of nano-scale pore attributes of Barakar Formation gas shales from Raniganj and Wardha Basin, India using low pressure sorption and FEG-SEM analysis. *J. Nat. Gas Sci. Eng.* **2020**, *81*, No. 103453.
(10) Holmes, R.; Aljamaan, H.; Vishal, V.; Wilcox, J.; Kovscek, A. R. Idealized Shale Sorption Isotherm Measurements to Determine Pore Capacity, Pore Size Distribution, and Surface Area. *Energy Fuels* **2019**, *33*, 665−676.
(11) Mastalerz, M.; Schimmelmann, A.; Drobniak, A.; Chen, Y. Porosity of Devonian and Mississippian New Albany Shale across a maturation gradient: Insights from organic petrology, gas adsorption, and mercury intrusion. *AAPG bulletin.* **2013**, *97* (10), 1621−43.
(12) Mastalerz, M.; Hampton, L. B.; Drobniak, A.; Loope, H. Significance of Analytical Particle Size in Low-Pressure N_2 and CO_2 Adsorption of Coal and Shale. *Int. J. Coal Geol.* **2017**, *178*, 122−131.
(13) Rouquerol, F.; Rouquerol, J.; Sing, K. S. W.; Llewellyn, P.; Maurin, G. *Adsorption by Powders and Porous Solids*; Elsevier: Amsterdam, The Netherlands, 2014.
(14) Jiang, Y.; Luo, Y.; Lu, Y.; Qin, C.; Liu, H. Effects of supercritical CO2 treatment time, pressure, and temperature on microstructure of shale. *Energy.* **2016**, *97*, 173−181.
(15) Huang, X.; Zhao, Y. P.; Wang, X.; Pan, L. Adsorption-induced pore blocking and its mechanisms in nanoporous shale due to interactions with supercritical CO2. *J. Pet. Sci. Eng.* **2019**, *178*, 74−81.
(16) Rani, S.; Padmanabhan, E.; Bakshi, T.; Prusty, B. K.; Pal, S. K. CO2 sorption and rate characteristics in micropores of shales. *J. Nat. Gas Sci. Eng.* **2019**, *68*, No. 102903.
(17) Hazra, B.; Wood, D. A.; Vishal, V.; Singh, A. K. Pore characteristics of distinct thermally mature shales: influence of particle size on low-pressure CO_2 and N_2 adsorption. *Energy Fuels.* **2018**, *32*, 8175−8186.
(18) Zhang, T.; Ellis, G. S.; Ruppel, S. C.; Milliken, K.; Yang, R. Effect of Organic-Matter Type and Thermal Maturity on Methane Adsorption in Shale-Gas Systems. *Org. Geochem.* **2012**, *47*, 120−131.
(19) Chandra, D.; Vishal, V.; Bahadur, J.; Agrawal, A. K.; Das, A.; Hazra, B.; Sen, D. Nano-scale physicochemical attributes and their impact on pore heterogeneity in shale. *Fuel* **2022**, *314*, No. 1203070.
(20) Bahadur, J.; Chandra, D.; Das, A.; Vishal, V.; Agrawal, A. K.; Sen, D. Pore anisotropy in shale and its dependence on thermal maturity and organic carbon content: A scanning SAXS study. *Int. J. Coal Geol.* **2023**, *273*, No. 104268.
(21) Curtis, M. E.; Ambrose, R. J.; Sondergeld, C. H.; Rai, C. S.. Investigation of the relationship between organic porosity and thermal maturity in the Marcellus Shale. In *SPE Unconventional Resources Conference/Gas Technology Symposium*, SPE 2011, SPE-144370-MS. DOI: .
(22) Hazra, B.; Wood, D. A.; Vishal, V.; Varma, A. K.; Sakha, D.; Singh, A. K. Porosity Controls and Fractal Disposition of Organic-Rich Permian Shales Using Low-Pressure Adsorption Techniques. *Fuel* **2018**, *220*, 837−848.
(23) Saidian, M.; Kuila, U.; Godinez, L. J.; Rivera, S.; Prasad, M. A Comparative Study of Porosity Measurement in Murdock. In *Society of Exploration Geophysicists International Exposition and 84th Annual Meeting*, SEG 2014, 2433−2438. DOI: .
(24) Yang, R.; Hu, Q.; Yi, J.; Zhang, B.; He, S.; Guo, X.; Hou, Y.; Dong, T. The Effects of Mineral Composition, TOC Content and Pore Structure on Spontaneous Imbibition in Lower Jurassic Dongyuemiao Shale Reservoirs. *Mar. Pet. Geol.* **2019**, *109*, 268−278.
(25) Chandra, D.; Bakshi, T.; Vishal, V. Thermal effect on pore characteristics of shale under inert and oxic environments: Insights on pore evolution. *Microporous Mesoporous Mater.* **2021**, *316*, No. 110969.
(26) Hazra, B.; Chandra, D.; Lahiri, S.; Vishal, V.; Sethi, C.; Pandey, J. K. Pore evolution during combustion of distinct thermally mature shales: Insights into potential in situ conversion. *Energy Fuels* **2023**, *37*, 13898−13911.
(27) Chandra, D.; Bakshi, T.; Bahadur, J.; Hazra, B.; Vishal, V.; Kumar, S.; Sen, D.; Singh, T. N. Pore morphology in thermally-treated shales and its implication on CO_2 storage applications: A gas sorption, SEM, and small-angle scattering study. *Fuel* **2023**, *331*, No. 125877.
(28) Chalmers, G. R.; Bustin, R. M.; Power, I. M. Characterization of gas shale pore systems by porosimetry, pycnometry, surface area, and field emission scanning electron microscopy/transmission electron microscopy image analyses: Examples from the Barnett, Woodford, Haynesville, Marcellus, and Doig units. *AAPG Bull.* **2012**, *96* (6), 1099−1119.
(29) Liu, X.; Xiong, J.; Liang, L. Investigation of Pore Structure and Fractal Characteristics of Organic-Rich Yanchang Formation Shale in Central China by Nitrogen Adsorption/Desorption Analysis. *J. Nat. Gas Sci. Eng.* **2015**, *22*, 62−72.
(30) Loucks, R. G.; Reed, R. M.; Ruppel, S. C.; Hammes, U. Spectrum of pore types and networks in mudrocks and a descriptive classification for matrix-related mudrock pores. *AAPG Bull.* **2012**, *96* (6), 1071−1098.
(31) Tian, H.; Pan, L.; Xiao, X. M.; Wilkins, R. W. T.; Meng, Z. P.; Huang, B. J. A preliminary study on the pore characterization of Lower Silurian black shales in the Chuandong Thrust Fold Belt, southwestern China using low-pressure N_2 adsorption and FE-SEM methods. *Mar. Pet. Geol.* **2013**, *48*, 8−19.
(32) Vishal, V.; Chandra, D.; Bahadur, J.; Sen, D.; Hazra, B.; Mahanta, B.; Mani, D. Interpreting Pore Dimensions in Gas Shales Using a Combination of SEM Imaging, Small-Angle Neutron Scattering, and Low-Pressure Gas Adsorption. *Energy Fuels* **2019**, *33*, 4835−4848.
(33) Xiong, J.; Liu, X.; Liang, L. Experimental study on the pore structure characteristics of the Upper Ordovician Wufeng Formation shale in the southwest portion of the Sichuan Basin, China. *J. Nat. Gas Sci. Eng.* **2015**, *22*, 530−384.
(34) Chandra, D.; Vishal, V. A critical review on pore to continuum scale imaging techniques for enhanced shale gas recovery. *Earth-Science Rev.* **2021**, *217*, No. 103638.
(35) Mandelbrot, B. B. *The fractal geometry of nature/Revised and enlarged edition/*. W.H. Freeman and Co: New York, 1983.
(36) Holmes, R.; Rupp, E. C.; Vishal, V.; Wilcox, J. Selection of Shale Preparation Protocol and Outgas Procedures for Applications in Low-Pressure Analysis. *Energy Fuels* **2017**, *31*, 9043−9051.
(37) Liu, K.; Ostadhassan, M.; Jang, H. W.; Zakharova, N. V.; Shokouhimehr, M. Comparison of Fractal Dimensions from Nitrogen

https://doi.org/10.1021/acsomega.4c07214
ACS Omega 2025, 10, 4395−4405

Adsorption Data in Shale: Via Different Models. *RSC Adv.* **2021**, *11*, 2298−2306.
(38) Zhang, S.; Tang, S.; Tang, D.; Huang, W.; Pan, Z. Determining Fractal Dimensions of Coal Pores by FHH Model: Problems and Effects. *J. Nat. Gas Sci. Eng.* **2014**, *21*, 929−939.
(39) Zhang, K.; Cheng, Y.; Jin, K.; Guo, H.; Liu, Q.; Dong, J.; Li, W. Effects of Supercritical CO_2 Fluids on Pore Morphology of Coal: Implications for CO_2 Geological Sequestration. *Energy Fuels* **2017**, *31*, 4731−4741.
(40) Yu, S.; Bo, J.; Fengli, L.; Jiegang, L. Structure and Fractal Characteristic of Micro- and Meso-Pores in Low, Middle-Rank Tectonic Deformed Coals by CO_2 and N_2 Adsorption. *Microporous Mesoporous Mater.* **2017**, *253*, 191−202.
(41) Wang, R. Y.; Gu, Y.; Ding, W. L.; Gong, D. J.; Yin, S.; Wang, X. H.; Zhou, X. H.; Li, A.; Xiao, Z. K.; Cui, Z. X. Characteristics and dominant controlling factors of organic-rich marine shales with high thermal maturity: A case study of the Lower Cambrian Niutitang Formation in the Cen'gong block, southern China. *J. Nat. Gas Sci. Eng.* **2016**, *33*, 81−96.
(42) Hazra, B.; Chandra, D.; Singh, A. K.; Varma, A. K.; Mani, D.; Singh, P. K.; Boral, P.; Buragohain, J. Comparative pore structural attributes and fractal dimensions of Lower Permian organic-matter-bearing sediments of two Indian basins: Inferences from nitrogen gas adsorption. *Energy Sources* **2019**, *41*, 2975−2988.
(43) Kumar, S.; Chandra, D.; Hazra, B.; Vishal, V.; Gamage, R. P. Nanopore characteristics of Barakar Formation shales and their impact on the gas storage potential of Korba and Raniganj Basins in India. *Energy Fuels* **2024**, *38*, 3833−3847.
(44) Vishal, V.; Verma, Y.; Chandra, D.; Ashok, D. A systematic capacity assessment and classification of geologic CO_2 storage systems in India. *Int. J. Greenhouse Gas Control* **2021**, *111*, No. 103458.
(45) Hazra, B.; Vishal, V.; Sethi, C.; Chandra, D. Impact of supercritical CO_2 on shale reservoirs and its implication for CO_2 sequestration. *Energy Fuels* **2022**, *36*, 9882−9903.
(46) Coal India Limited *Coal Atlas of India*, Central Mine Planning & Design Institute: Calcutta, India, 1993.
(47) Ahuja, M.; Mishra, D. P.; Mohanty, D.; Agrawal, H.; Roy, S. Development of Empirical and Artificial Neural Network Model for the Prediction of Sorption Time to Assess the Potential of CO2 Sequestration in Coal. *ACS omega.* **2023**, *8* (34), 31480−92.
(48) Rietveld, H. M. Line profiles of neutron powder-diffraction peaks for structure refinement. *Acta Crystallogr.* **1967**, *22*, 151−152.
(49) Hazra, B.; Singh, D. P.; Chakraborty, P.; Singh, P. K.; Sahu, S. G.; Adak, A. K. Using Rock-Eval S4Tpeak as Thermal Maturity Proxy for Shales. *Mar. Pet. Geol.* **2021**, *127*, No. 104977.
(50) Hazra, B.; Dutta, S.; Kumar, S. TOC Calculation of Organic Matter Rich Sediments Using Rock-Eval Pyrolysis: Critical Consideration and Insights. *Int. J. Coal Geol.* **2017**, *169*, 106−115.
(51) Han, H.; Cao, Y.; Chen, S. J.; Lu, J. G.; Huang, C. X.; Zhu, H. H.; Zhan, P.; Gao, Y. Influence of Particle Size on Gas-Adsorption Experiments of Shales: An Example from a Longmaxi Shale Sample from the Sichuan Basin. *China. Fuel* **2016**, *186*, 750−757.
(52) Wei, M.; Xiong, Y.; Zhang, L.; Li, J.; Peng, P. The Effect of Sample Particle Size on the Determination of Pore Structure Parameters in Shales. *Int. J. Coal Geol.* **2016**, *163*, 177−185.
(53) Yang, C.; Xiong, Y.; Zhang, J. A. Comprehensive Re-Understanding of the OM-Hosted Nanopores in the Marine Wufeng− Longmaxi Shale Formation in South China by Organic Petrology, Gas Adsorption, and X-Ray Diffraction Studies. *Int. J. Coal Geol.* **2020**, *218*, No. 103362.
(54) Singh, D. P.; Chandra, D.; Vishal, V.; Hazra, B.; Sarkar, P. Impact of Degassing Time and Temperature on the Estimation of Pore Attributes in Shale. *Energy Fuels* **2021**, *35*, 15628.
(55) Kuila, U.; Prasad, M. Specific surface area and pore-size distribution in clays and shales. *Geophys. Prospect.* **2013**, *61* (61), 341−362.
(56) Gentzis, T.; Carvajal-Ortiz, H.; Tahoun, S. S.; Deaf, A.; Ocubalidet, S. Organic facies and hydrocarbon potential of the early-middle Albian Kharita Formation in the Abu Gharadig Basin, Egypt, as demonstrated by palynology, organic petrology, and geochemistry. *Int. J. Coal Geol.* **2019**, *209*, 27−39.
(57) Magoon, L. B.; Dow, W. G. Applied Source Rock Geochemistry: Chapter 5: Part II. Essential Elements. *AAPG* **1994**, *77*, 93−120.
(58) Hunt, J. M. *Petroleum geochemistry and geology*, 2nd ed.; W.H. Freeman and Company: New York, 1996, 743.
(59) Groen, J. C.; Peffer, L. A. A.; Pérez-Ramírez, J. Pore size determination in modified micro- and mesoporous materials. Pitfalls and limitations in gas adsorption data analysis. *Microporous Mesoporous Mater.* **2003**, *60*, 1−17.
(60) Avnir, D.; Farin, D.; Pfeifer, P. Molecular fractal surfaces. *Nature* **1984**, *308* (5956), 261.
(61) Pfeifer, P.; Wu, Y. J.; Cole, M. W.; Krim, J. Multilayer adsorption on a fractally rough surface. *Phys. Rev. Lett.* **1989**, *62* (17), 1997.
(62) Yang, R.; Hao, F.; He, S.; He, C. C.; Guo, X. S.; Yi, J. Z.; Hu, H. Y.; Zhang, S. W.; Hu, Q. H. Experimental investigations on the geometry and connectivity of pore space in organic-rich Wufeng and Longmaxi shales. *Mar. Pet. Geol.* **2017**, *84*, 225−242.
(63) Xi, Z. D.; Tang, S. H.; Zhang, S. H.; Sun, K. Pore structure characteristics of marine continental transitional shale: A case study in the Qinshui Basin. *China. Energy Fuels* **2017**, *31*, 7854−7866.
(64) Li, Z.; Zhang, J.; Mo, X.; Tong, Z.; Wang, X.; Wang, D.; Su, Z.; Tang, X.; Gong, D. Characterization of an Angstrom-Scale Pore Structure in Organic-Rich Shales by Using Low-Pressure CO_2Adsorption and Multifractal Theory and Its Role in CH_4/CO_2Gas Storage. *Energy Fuels* **2022**, *36*, 12085−12103.
(65) Xu, Z.; Shi, W.; Zhai, G.; Peng, N.; Zhang, C. Study on the characterization of pore structure and main controlling factors of pore development in gas shale. *Journal of Natural Gas Geoscience* **2020**, *5*, 255−271.

https://doi.org/10.1021/acsomega.4c07214
ACS Omega 2025, 10, 4395−4405